Bulletin of the Seismological Society of America, 90, 4, pp. 914–928, August 2000

Envelope Broadening of Outgoing Waves in 2D Random Media: A Comparison between the Markov Approximation and Numerical Simulations

by Michael Fehler, Haruo Sato, and Lian-Jie Huang

Abstract Observations of seismic waves from earthquakes at depths between 100 and 200 km beneath Japan show that the initial portion of the *S*-wave arrival has greater duration than can be accounted for by earthquake source-time duration. The observed long duration of *S* waves has been explained as being caused by multiple forward scattering around the ray path between source and receiver. Array observations of *Lg* waveforms have also shown that multiple forward scattering along the path between the source and receiver are important influences on the character of *Lg* waveforms and that the scattering cannot be explained only by vertical variations in velocity. Multiple forward scattering in 3D has been modeled using the Markov approximation for the parabolic-wave equation, which allows the calculation of seismogram envelopes in statistically characterized random media. To test the range of validity of the Markov approximation-derived solutions, we made 2D numerical calculations of wavefields in random media using approximations to the parabolic wave equation, which only models forward scattering, and by finite-difference solution of the scalar-wave equation, which gives complete wavefields. Media of background velocity 4 km/sec are characterized using a Gaussian autocorrelation function with a 5 km correlation distance and 5% rms fractional fluctuation. To compare with envelopes obtained from the Markov approximation, we calculated wavefields for source-receiver distances ranging from 50 to 200 km for several statistically identical realizations of random media. We obtain ensemble average envelopes by averaging envelopes from the realizations. We find a good agreement between ensemble-average envelopes obtained from the numerical solution of the parabolic-wave equation and envelopes obtained from the Markov approximation. The later portion of the ensemble-average envelopes calculated using finite difference have larger amplitudes than those from the Markov approximation, which is probably due to the late-arriving energy that has been scattered at wide angles from the global propagation direction between the source and the receiver. We observe that the variations among the numerically calculated envelopes of individual realizations of random media are well fit by a Rayleigh distribution, which describes the distribution of envelope amplitude when signals of one frequency but random phase are summed. Our results show that the Markov approximation provides reliable information about envelope shapes for forward-scattered wavefields but that the influence of wide-angle scattering and backscattering have some influences on envelope shapes and should be considered when analyzing data using random media models.

Introduction

Seismograms of regional earthquakes contain phases that cannot be readily explained using deterministic models of the Earth. Aki (1969) first proposed that latter portions of seismograms may be explained as being caused by scattering of waves from randomly distributed heterogeneities located within the vicinity of the source-receiver path. Since Aki's proposal, numerous observations and models have been made to characterize the heterogeneity within the Earth's lithosphere. A summary of observations and models can be found in Sato and Fehler (1998) and Shapiro and Hubral

(1999). Here, we focus on seismic-wave propagation over regional distances (greater than 50 km) and the early portion of observed seismograms so that we can consider the influences of forward scattering on the character of observed data.

Forward-scattering models have been used to interpret phase and amplitude variations observed on seismic arrays since the early 1970s using the methods derived from the work of Chernov (1960) and more recently by Flatté and Wu (1988). Sato (1989) investigated the character of individual *S* waves on seismograms recorded at regional distances from deep earthquakes under Japan. He noted that the initial portion of the *S*-wave-arrival packet extends over a longer time period (several seconds) than could be explained by source effects. He called this phenomenon envelope broadening. He numerically characterized the shape of the packet in the 2–32 Hz band as a function of distance to approximately 300 km using two parameters: (1) the envelope duration time, which is the time between the *S*-wave arrival and when the envelope decreases to half of its maximum amplitude, and (2) the difference in time between the *S* arrival and when the peak in the envelope occurs. Sato (1989) proposed that forward scattering around the path between the source and receiver could explain his observations. He used the parabolic approximation to the wave equation, which models forward wave propagation, and the Markov approximation to explain his observations. His source was a quasi-monochromatic plane-wave incident onto an inhomogeneous medium from a homogeneous one. Using a Gaussian spectral description of the heterogeneity, Sato (1989) modeled his observations and inferred the statistical properties of the random heterogeneity along the source-receiver paths used in his observations. Scherbaum and Sato (1991) analyzed a large dataset using an inversion method to improve the estimation of media parameters inferred using Sato's (1989) model. Subsequently, Obara and Sato (1995) analyzed data from a larger region in Japan and showed that the characteristics of the seismogram envelopes measured by Sato (1989) varied systematically with tectonic province.

Other observations showing the importance of forward scattering on the character of regional seismograms include those on *Lg* by Der *et al.* (1984) and Dainty and Toksöz (1990), who showed that the early portion of *Lg* is dominated by forward-scattered energy. Wagner (1997) analyzed waveforms of earthquakes in Southern California and Nevada using a seismic array and showed that the initial portions of the *P*- and *S*-wave packets consist of forward scattered energy and relatively little mode conversion.

Numerical modeling of wave propagation in random media has been undertaken by numerous seismologists. Frankel and Clayton (1986) investigated the influences of scattering on seismograms of local earthquakes using 2D finite-difference (FD) modeling. Ikelle *et al.* (1993) used 2D FD modeling to investigate the influences of anisotropy in the heterogeneity of random media on pulse broadening, coda formation, and apparent anisotropy. They chose a scale appropriate for petroleum exploration and found that pulse broadening is relatively independent of the degree of anisotropy in the heterogeneity but that coda formation and apparent anisotropy were greatly influenced by the amount of anisotropy in the heterogeneity.

Shapiro and Kneib (1993) investigated diffraction effects on predicted amplitudes of first arrivals using the parabolic approximation and discussed the difference between individual simulations and ensemble averages of simulations. Travel times through random media with characteristics appropriate for the Earth have been investigated by Müller *et al.* (1992) and Roth *et al.* (1993). Müller *et al.* (1992) presented a theory for analyzing traveltimes in random media and used waveforms generated by FD simulations of acoustic-wave propagation to compare travel times with medium properties. They discussed how statistical properties such as mean-velocity fluctuation and scale length of fluctuation may be estimated from measured travel-time data.

Gusev and Abubakirov (1996) used Monte Carlo simulations of the energy transport equation (Ishimaru, 1978) to investigate waveform envelopes at locations both near and far from a source. Their goal was to investigate the types of random media that could explain the observation of coda near the source and envelope broadening at large distance from the source. They noted the inconsistency between models used to explain near-source coda amplitudes and those used to explain envelope broadening at large distances. Strong forward-scattering models have been used to explain envelope broadening at large propagation distances; however, these models predict little coda in the near-source region, which is contrary to observations. Gusev and Abubakirov (1996) propose that using a power-law characterization of medium heterogeneity results in both near-source coda and envelope broadening at large distances.

We investigate the accuracy of approximate techniques for modeling 2D forward-wave propagation in random media against more exact full-wave numerical techniques. We compare mean envelopes calculated at regional distances in the Earth using two approaches for one-way wave propagation with envelopes obtained using FD of the scalar-wave (constant density) equation. We model one-way wave propagation using the Markov approximation of the 2D parabolic-wave equation, which is an extension of the method of Shishov (1974) for modeling the broadening of spherically outgoing wave envelopes and for modeling the broadening of plane wave envelopes in 3D (Lee and Jokipii, 1975a, b; Sreenivasiah *et al.,* 1976; Sato, 1989). In contrast to previous studies using the Markov approximation, our source is a point source in space with a Ricker wavelet time history, which has a finite bandwidth. The source is located within the heterogeneous medium. We also model one-way wave propagation using a numerical method based on the Rytov approximation and the use of a one-way Green Function. This numerical method has been shown to be a reliable propagator for migration by Huang *et al.* (1999). Finally, we

use FD modeling of the scalar-wave equation to obtain waveforms that include reverberations, which are not included in the one-way propagation methods. Our goal is to compare the three methods, investigate their reliability, and to determine what features in seismogram envelopes are different between those calculated using one-way modeling approaches and those resulting from full-wavefield approaches, which model both forward propagation as well as reverberations within the media. We choose 2D random media to reduce computational cost and allow enough computations to be conducted to make a stable estimate of envelope shape using many realizations.

Random Media

We study forward wave propagation in 2D random media. Forward scattering dominates when the wavelength is less than the characteristic length of heterogeneity of the media (Sato and Fehler, 1998). We choose random media where departure from some average velocity V_0 is described using an autocorrelation function. To obtain average statistical properties of the wavefield, we must consider an ensemble of random media $\{\chi(\mathbf{x})\}$ having identical autocorrelation functions (Sato and Fehler, 1998). We write velocity as

$$V(\mathbf{x}) \equiv V_0 + \delta V(\mathbf{x}) = V_0(1 + \xi(\mathbf{x})) \tag{1}$$

where $\xi(\mathbf{x})$ is the fractional fluctuation of wave velocity, and V_0 is the mean velocity such that

$$V_0 = \langle V(\mathbf{x}) \rangle \text{ and } \langle \xi(\mathbf{x}) \rangle = 0 \tag{2}$$

where the angular brackets mean the ensemble average. We define the autocorrelation function (ACF) of the medium as

$$R(\mathbf{x}) \equiv \langle \xi(\mathbf{y}) \xi(\mathbf{y} + \mathbf{x}) \rangle \tag{3}$$

The ACF function is a statistical measure of the spatial scale and magnitude of the fluctuation of media properties. We choose media with ACF that are independent of $\mathbf{y}$ and are a function of lag vector $\mathbf{x}$ only. This means that the medium is statistically homogeneous. The magnitude of the fractional fluctuation is given by the mean square (MS) fractional fluctuation:

$$\varepsilon^2 \equiv R(0) = \langle \xi(\mathbf{y})^2 \rangle \tag{4}$$

There are many forms of ACF used to investigate random media (Sato and Fehler, 1998). We choose the Gaussian ACF for isotropic media because it is one that has been used in Earth wave-propagation studies and because it is one for which envelopes can be analytically obtained using the Markov approximation. The Gaussian ACF is given by:

$$R(\mathbf{x}) \equiv R(r) = \varepsilon^2 e^{-r^2/a^2} \tag{5}$$

where $r = |\mathbf{x}|$ and a is the correlation distance. To construct numerical realizations of random media having a given ACF, we note that the Fourier transform of the 2D ACF given in (5) is

$$P(\mathbf{m}) \equiv F\{R(\mathbf{x})\} \equiv P(m) = \varepsilon^2 \pi a^2 e^{-m^2 a^2/4} \tag{6}$$

where $F\{\ \}$ represents Fourier transform over 2D space, $\mathbf{m}$ is the Fourier transform variable, and $m = |\mathbf{m}|$. To generate a random medium, we construct a function that has the power spectra given by (6), take the square root, and randomize its phase. We taper for values of $m > m_{\max}/2$ to reduce aliasing effects, take the inverse Fourier transform into the space domain, and get $\xi(\mathbf{x})$. Figure 1 shows an example of a Gaussian random medium whose correlation distance a is 5 km and fractional fluctuation ϵ is 0.05.

Models Used

We choose a model dimension to be large enough so that envelope broadening could be observed while limiting

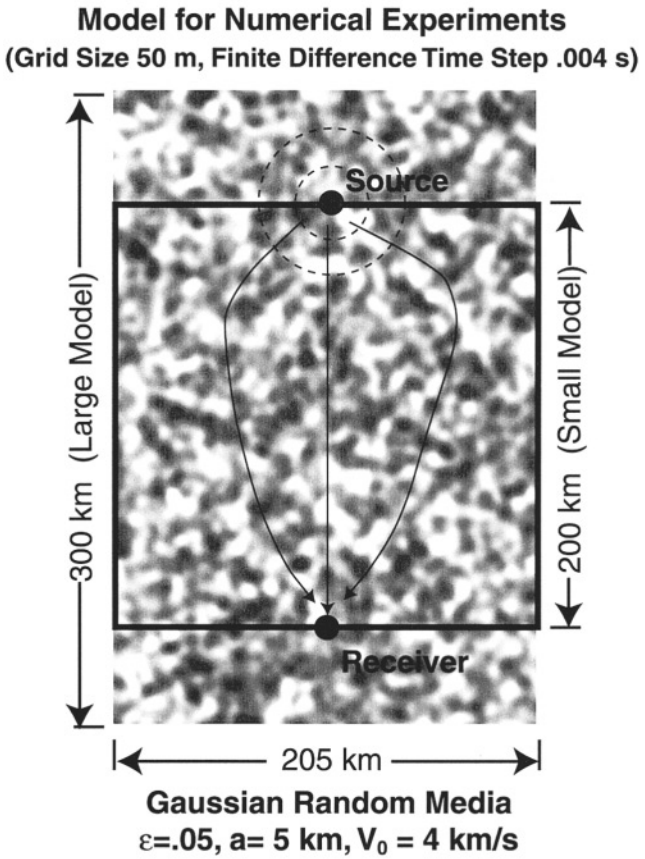

Figure 1. Random medium characterized by Gaussian autocorrelation function with correlation length of 5 km and fractional fluctuation of 5%. Geometries of large and small models are shown. Large model is 300 by 205 km; small model is 200 by 205 km. Source and receiver are located equidistant from lateral boundaries.

the model size to limit time required for numerical calculations. Maximum source-receiver distance is 200 km, and the source is a Ricker wavelet with a central frequency of 2 Hz. Background medium velocity is 4 km/sec, which gives a dominant wavelength of 2 km. Correlation length is 5 km, which ensures that forward scattering dominates. The value of ε was selected to be 0.05, which keeps minimum and maximum velocities within a range required for reliable numerical wavefield calculations.

Our calculations were conducted using two model geometries. The extended local Rytov Fourier (ELRF) and Markov approximation methods model one-way wave propagation and do not include backscattering. Without backscattering, the only region that needs to be modeled is the region between by the source and receiver along the propagation direction. The model width was selected to ensure that the initial arrival packet at the receiver has no influences from waves reflected from lateral boundaries. Thus, one model geometry, the small model, is 200 km long and 205 km wide. The source was placed in the center of one side of the model and the most distant receiver at the center of the opposite side. Model geometry, including locations of source and most distant receiver are shown in Figure 1. The travel time for a direct arrival from the source to the receiver at 200 km in the background medium is 50 sec and the time for a pulse to travel from the source to the lateral boundary and then to the receiver is 71.6 sec, so we conclude that at least the initial 20 sec of the first arriving wave packet at 200 km distance has no influence from reflections off the model side boundaries. To evaluate the influences of scattering in the near-source and near-receiver regions, we also used a model of length 300 km and width 205 km (Fig. 1). This model is called the large model. In this model there is 50 km between the source location and the nearest boundary of the model and 50 km between the most distant receiver and the nearest model boundary, which allows reverberations in the vicinity of the source and the most distant receiver. Boundary reflections from the near-source and near-receiver regions should not arrive until 25 sec after the direct arrival in background medium.

Numerical Modeling Methods

Numerical modeling is undertaken using two methods. One method is FD modeling of the scalar-wave equation. The other is a procedure for modeling one-way wave propagation, the ELRF modeling approach. We will now discuss these methods.

Finite-Difference Modeling

Finite-difference modeling is accomplished with a 2D FD code that has fourth-order accuracy in space and second-order accuracy in time. The code uses Holberg coefficients (Holberg, 1987), which are optimal for minimizing grid dispersion for a given number of grid points per wavelength. We use Higdon absorbing boundaries (Higdon, 1991).

In FD modeling, we wish to have small grid dispersion over the propagation distance being modeled. For modeling to distances of a few wavelengths from the source, a grid spacing giving 7–10 gridpoints per wavelength is sufficient to limit grid dispersion. However, our study requires modeling to distances of 100 wavelengths from the source so the number of gridpoints required per wavelength is 40. We thus used grid spacing of 50 m and time step of 4 msec. Figure 2 shows waveforms as a function of distance for waves propagating in a homogeneous medium calculated using our FD scheme. The top portion of Figure 2 shows the result obtained using a grid spacing of 200 m and time step of 40 msec. The bottom portion of Figure 2 shows the result obtained when using a grid spacing of 50 m and time step of 4 msec. The figure clearly shows the waveform distortion when the larger grid spacing is used. The distortion is dominated by the highest frequencies in the source pulse.

Extended Local Rytov Fourier Method

The ELRF modeling method uses the Rytov approximation for modeling one-way wave propagation in hetero-

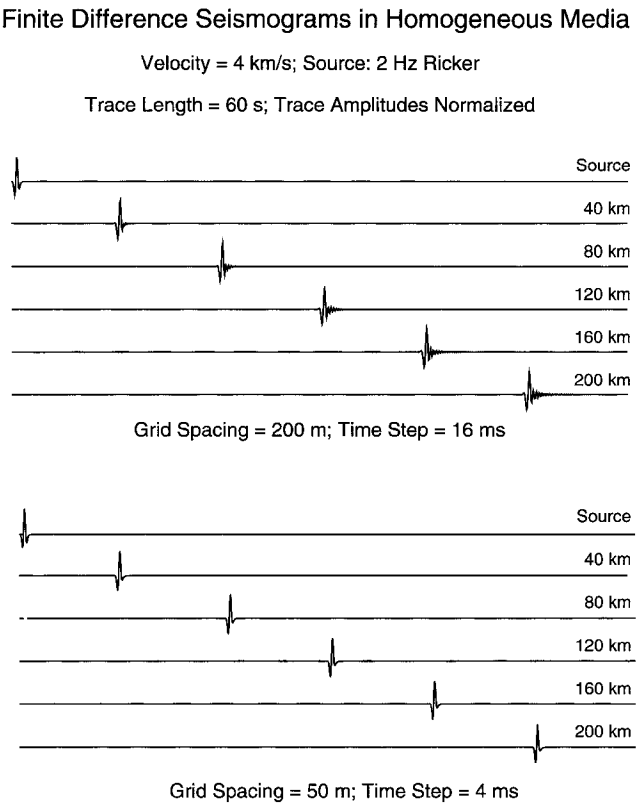

Figure 2. Finite-difference calculations of wave propagation in homogeneous media with velocity of 4 km/sec. Source is 4-Hz Ricker wavelet. Upper traces were calculated using grid spacing of 200 m or 10 gridpoints per wavelength at 2 Hz. Note clear dispersion at distances greater than about 40 km. Lower traces were calculated using 50-m grid spacing or 40 gridpoints per wavelength at 2 Hz. There is no observable grid dispersion for these traces.

geneous media (Huang *et al.,* 1999). The method is similar to the split-step Fourier (SSF) method that has been used in acoustics for modeling wave propagation in random media (Jensen *et al.,* 1994), and by the petroleum industry for migration (Stoffa *et al.,* 1990). The reliability of the SSF method is discussed in Huang and Fehler (1998). The ELRF has a wider range of reliability than the SSF method and has been shown to give better images than the SSF method when used to migrate post and prestack datasets of interest to the petroleum industry (Huang *et al.,* 1999).

Propagation of scalar wave $u(\mathbf{x}, t)$ through 2D random media is governed by the wave equation:

$$\left(\Delta - \frac{1}{V(\mathbf{x})^2}\,\partial_t^2\right) u(\mathbf{x},t) = 0 \tag{7}$$

where $\mathbf{x} = (x, z)$ and $\Delta = \partial^2/\partial x^2 + \partial^2/\partial z^2$ is the Laplacian operator in 2D. Substituting (1) into (7), we can rewrite (7) in the case that $|\xi| \ll 1$ as

$$\left(\Delta - \frac{1}{V_0^2}\,\partial_t^2\right) u(\mathbf{x},t) + \frac{2}{V_0^2}\,\xi(\mathbf{x})\partial_t^2 u(\mathbf{x},t) = 0 \tag{8a}$$

The ELRF method uses a one-way Green Function to model propagation across layers perpendicular to the global propagation direction. Huang *et al.* (1999) derive the propagation equations from the angular-frequency domain form of (8a)

$$\left(\Delta + \frac{\omega^2}{V_0^2}\right) u(\mathbf{x},\omega) = 2\,\frac{\omega^2}{V_0^2}\,\xi(\mathbf{x})u(\mathbf{x},\omega) \tag{8b}$$

At a source-receiver distance r, which is longer than the wavelength ($r \gg 1/k_0$) and correlation distance ($r \gg a$), we may write the outgoing wave radiated from a source at the origin using the Fourier transform with respect to time as

$$u(r,\theta,t) = \frac{1}{2\pi}\int_{-\infty}^{\infty} d\omega\,\frac{U(r,\theta,\omega)}{\sqrt{k_0 r}}\,e^{i(k_0 r - \omega t)} \tag{9}$$

where wavenumber $k_0 = \omega/V_0$, θ is the polar angle, and $U(r,\theta,\omega)$ is the amplitude of an outgoing harmonic wave. Substituting (9) in (8a), we get the wave equation in polar coordinates as

$$\left(\partial_r^2 U + 2ik_0\partial_r U + \frac{U}{4r^2} - k_0^2 U + \frac{\partial_\theta^2 U}{r^2}\right) + k_0^2 U - 2k_0^2\xi U = 0 \tag{10}$$

When $a \gg 1/k_0$, the amplitude U changes very slowly with travel distance; therefore, we may neglect the first term in (10). We may neglect the third term since $r \gg 1/k_0$. Thus, we obtain the parabolic wave equation for U:

$$2ik_0\partial_r U + \frac{\partial_\theta^2 U}{r^2} - 2k_0^2\xi U = 0 \tag{11}$$

This is the equation governing one-way wave propagation in polar coordinates and its counterpart in Cartesian coordinates can be used to derive the SSF method (Huang and Fehler, 1998).

To derive the propagation equations for the one-way ELRF method, we write the wavefield $u(\mathbf{x},\omega)$ in (8b) as the product of two terms,

$$u(\mathbf{x},\omega) = e^{\phi_0(x,\omega) + \phi_s(x,\omega)} \tag{12}$$

where $u_0(\mathbf{x},\omega) = e^{\phi_0(\mathbf{x},\omega)}$ is the wavefield at $\mathbf{x}$ obtained by propagation through a homogeneous background medium having some average velocity and $u_s(\mathbf{x},\omega) = e^{\phi_s(\mathbf{x},\omega)}$ is a term to correct the wavefield for the heterogeneity of the medium. Note that $\varphi_0(\mathbf{x},\omega)$ and $\varphi_s(\mathbf{x},\omega)$ are complex.

For one-way wave propagation, Huang *et al.* (1999) showed that the wavefield at some depth z_{i+1} may be calculated from knowledge of the wavefield at z_i using

$$u(x,z_{i+1};\omega) = u_0(x,z_{i+1};\omega)e^{\phi_s(x,z_{i+1};\omega)} \tag{13}$$

Wavefield $u_0(x, z_{i+1}; \omega)$ at z_{i+1} is obtained by propagation of the known wavefield at z_i across the interval $\Delta z = z_{i+1} - z_i$ where the interval is assumed to have homogeneous velocity V_0

$$u_0(x,z_{i+1};\omega) = F_{k_x}^{-1}\left\{e^{ik_z\Delta z}\,F_x\left\{u(x,z_i,\omega)\right\}\right\} \tag{14}$$

where $k_z = \sqrt{k_0^2 - k_x^2}$, $k_0 = \omega/V_0$, and F_x, $F_{k_x}^{-1}$ are Fourier and inverse Fourier transforms over x and k_x, respectively (note that Fourier transform over x gives k_x). The term in the exponential in (13) is calculated in the Rytov approximation as

$$\phi_s(x,z_{i+1};\omega) \equiv \psi(x,z_{i+1};\omega)/u_0(x,z_{i+1};\omega) \tag{15a}$$

where

$$\psi(x,z_{i+1};\omega) = F_{k_x}^{-1}\left\{\frac{k_0}{k_z}\,e^{ik_z\Delta z}\,F_x\left\{i\omega\Delta z\Delta s(x,z_i)u(x,z_i;\omega)\right\}\right\} \tag{15b}$$

where $\Delta s(x, z_i) = -\xi(x, z_i)/V(x, z_i)$ is the slowness perturbation, which is assumed to be smooth. Since the propagator depends only on the local properties of the medium, one does not have to have access to an entire model to propagate through a portion of the medium. This gives the method a great computational advantage over some other wave-equation based methods such as wave-equation FD. As discussed by Huang *et al.* (1999), the ELRF approach is stable, handles amplitudes reliably, and gives high-quality images when used to migrate data collected by the petroleum industry.

Numerical Modeling Results

Comparison of Finite Difference and Rytov Modeling Results

Wave equation FD modeling provides a reliable estimation of the entire wavefield because it includes all wave phenomena including reverberations. However, the computational cost of FD is significant compared to ELRF. Figure 3 shows traces calculated using FD and ELRF for identical models. Waveforms are shown at 25 km intervals between 50 and 200 km for one realization of the small model shown in Figure 1. The FD medium was padded on all edges to allow for nonreflecting boundaries. The source-time history is a Ricker function with central frequency of 2 Hz. The grid spacing for the FD and ELRF models was identical (50 m). The ELRF wavefield was calculated using 246 frequencies between 0.1 and 6.0 Hz. Figure 3 shows that the waveforms calculated using the two methods are nearly identical for the initial 10 sec after the first arrival at all distances modeled. For later times, the ELRF trace has small or zero amplitude since ELRF does not include reverberations within the medium, which are modeled using FD. The FD calculation took a factor of 25 times more CPU time and a factor of 3.5 times more memory than the ELRF calculation. The practical speed and memory differences between the methods are larger since the 50-m-grid interval was required by the FD method and the grid interval could be larger for the ELRF method.

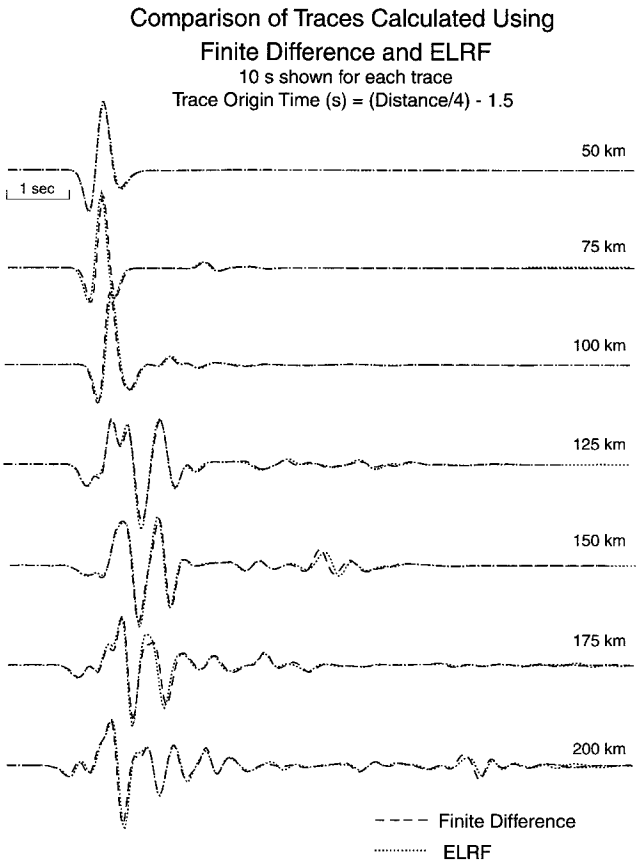

Figure 3. Waveforms calculated using FD and ELRD for propagation through a random medium. Source-receiver distance for each trace is shown above each trace.

Waveforms for individual random media

Waveforms were calculated for a total of 100 realizations of random media for three cases, finite difference of the small model, finite difference of the large model, and ELRF of the small model. There is considerable variation in waveform character among the various realizations. Figure 4 shows FD waveforms calculated for 15 realizations of the large model. Waveforms are shown at four source-receiver distances.

The changes in character as a function of propagation distance can be seen by comparing the figures for various distances. At a 50-km propagation distance (Fig. 4a), most waveforms look similar to the source pulse and few have later scattered arrivals. The differences among the waveforms at this distance are dominated by the variations in first-arrival times. Sato (1982) argued that these travel-time variations are caused by the long-wavelength component of the velocity heterogeneity. He showed how to remove the influences of these travel-time fluctuations in a calculation of the pulse-amplitude attenuation to arrive at a model for scattering attenuation that is in agreement with observations.

As propagation distance increases, waveforms become more complex as later arrivals lengthen the waveforms and even first-arrivals no longer resemble the source pulse. The differences among the waveforms at a given distance for various realizations of random media become significant even at a 100-km distance (Fig. 4b). At this distance, the first-arrival packet often does not contain the maximum amplitude of the entire waveform. At distances of 150 and 200 km (Fig. 4c,d), the maximum amplitude is seldom at the beginning of the waveform.

Figure 5a and b shows record corrections, corrected with a moveout velocity of 4 km/sec for two realizations of random media. These sections show clearly the increasing complexity of the waveform as propagation distance increases and the striking differences among the waveforms for the two realizations of random media.

Ensemble Average Envelopes

Average envelopes were calculated from a total of 100 realizations of random media to obtain ensemble average envelopes. Ensemble average envelopes were calculated by squaring waveforms from each realization, summing results from all realizations, taking the square root, and smoothing over a 0.32 second window.

Figure 6 shows ensemble-average envelopes at 200-km propagation distance calculated for three cases: (1) FD of small model (thin solid curve), (2) FD of large model (black solid curve), and (3) ELRF of small model (dotted curve). The figure shows that the envelopes obtained by FD and ELRF of the small model are nearly identical in their early

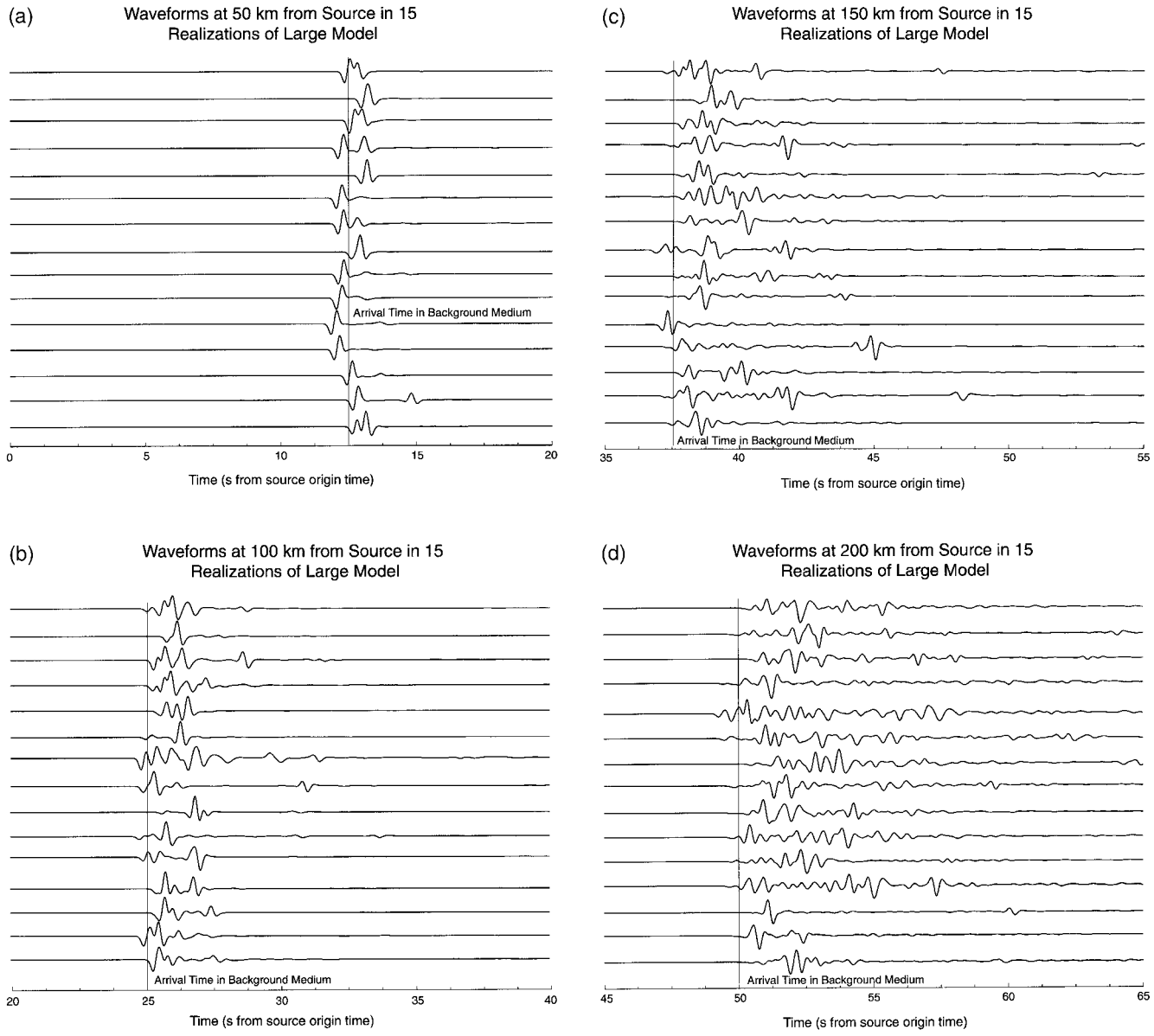

Figure 4. Waveforms obtained using FD for 15 realizations of large model. Note significant difference in waveform character among the realizations. (a) propagation distance of 50 km, (b) propagation distance of 100 km, (c) propagation distance of 150 km, (d) propagation distance of 200 km. Vertical lines indicate arrival time for constant velocity media with velocity equal to background velocity. Time scale is relative to source-origin time.

portion and begin to differ only after about 52 sec. The similarity of results obtained by the two methods is expected since the time-domain traces for individual realizations shown in Figure 3 are nearly identical. The one significant difference between the results from the two methods is that the envelope amplitude at times greater than about 55 sec is systematically larger when calculated using FD. This can be explained by the influences of reverberation, which is modeled correctly by FD but ignored in ELRF. The difference in late lapse-time envelope amplitudes shows that backscattering is small but significant.

The FD ensemble-average envelopes calculated for the small and large models are slightly different. We attribute the differences in overall shape of the envelopes for the two models to be due to the statistical variation of the ensemble average. Support for this conclusion comes from comparing waveforms in the time interval 45–55 sec at 200 km calculated using ELRF with those calculated using FD on the large model. Modeling of the large model with ELRF, which does not include backscattering, yielded almost identical waveforms to those calculated using FD on the large model. We thus conclude that the ensemble-average envelopes calcu-

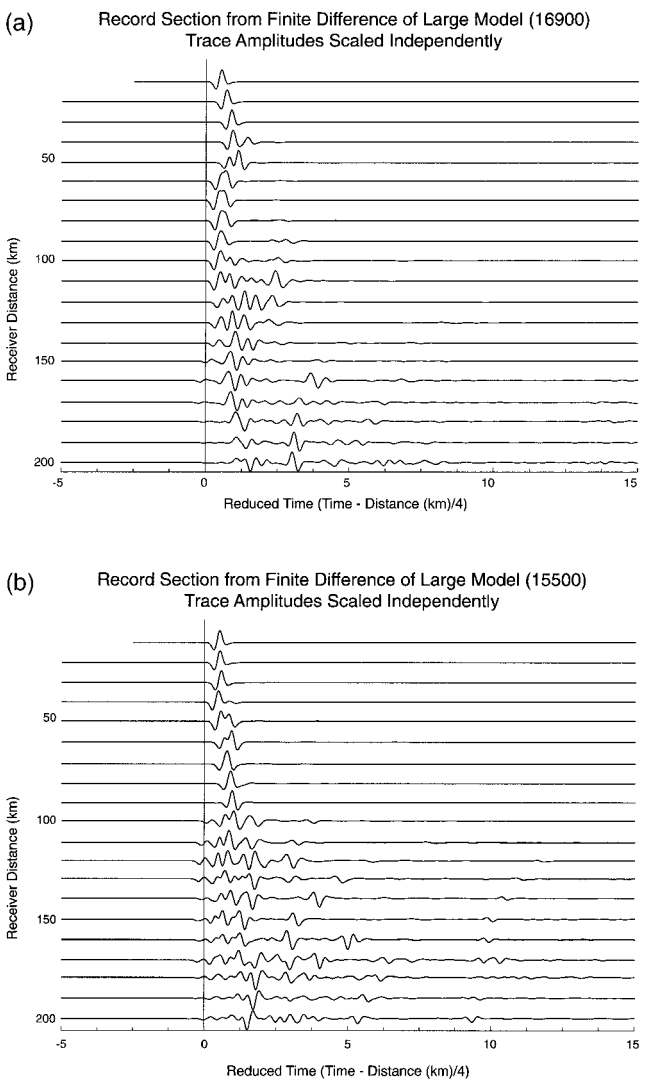

Figure 5. Record sections (waveforms vs. travel distance) for two realizations of large model calculated using FD. Traces have been shifted using a the background velocity as moveout velocity. Time scale is relative to source-origin time.

lated for the large model using ELRF would not differ significantly in the time period of 45 to about 55 sec from those calculated using FD.

Variations in Numerically-Calculated Ensemble Average Envelopes

Figure 7 shows histograms of ELRF trace amplitude of 100 individual traces at 12.5 sec at a distance of 50 km and 51.5 sec at a distance of 200 km. Histograms of envelope amplitudes for the 100 traces at the same time for each distance are also shown. Histograms of trace amplitudes appear to follow a normal distribution with zero mean. The distributions for envelope amplitudes do not appear to be described by a Gaussian distribution. The departure from a Gaussian distribution is not surprising because envelope amplitude cannot be less than zero.

The distribution of trace and envelope amplitudes for waveforms composed of a superposition of oscillations having the same frequency but random phase was studied by Rayleigh (1880) and later by Landon (1941, 1942). Landon (1942) shows that the distribution of instantaneous amplitudes of a waveform composed of a sum of waves of the same frequency but random phase is given by

$$P(\eta) \sim \frac{1}{\sigma\sqrt{2\pi}}\, e^{-\eta^2/2\sigma^2} \tag{16}$$

where η is amplitude and σ is the standard deviation of the distribution, and that the distribution of envelope amplitude E is given by

$$P(E) \sim \frac{E}{\sigma^2}\, e^{-E^2/2\sigma^2} \tag{17}$$

For these distributions, the most likely value of envelope amplitude is σ, the mean is 1.252σ, and the standard deviation of envelope amplitude is $.655\sigma$ (Landon, 1942). This means that the standard deviation of envelope amplitude is $.655\sigma = .655\bar{M}/1.242 = .527\bar{M}$ where $\bar{M}$ is the amplitude of the mean envelope.

Plotted in Figure 7 are curves corresponding to (16) and (17). Values of σ were determined from the amplitude histograms and used to plot the characteristic curves for the envelope histograms. The histograms are well-fit by the distributions given by (16) and (17). This may not be surprising since the waveforms are bandlimited and can be considered to be superpositions of scattered pulses of random phase.

Markov Approximation

The term Markov approximation as used by authors of work in forward scattering has its roots in the concept of Markov process, which is one where the probability of future events is dependent only on most recent events (Barabanenkov et al., 1971). Here we will calculate ensemble average envelopes for the case where forward scattering dominates. In this case, the wavefield can be extrapolated in time away from the source in a manner that the wavefield at some distance can be determined once the wavefield at some slightly smaller distance is known. Hence, we use the term Markov approximation.

Markov Approximation for the Quasi-monochromatic Waves in Random Media Characterized by a Gaussian ACF

We study the long travel distance propagation of quasi-monochromatic waves radiated from a point source. Instead of modeling individual waveforms, we model envelope shape. We will use the parabolic equation (11) to derive a

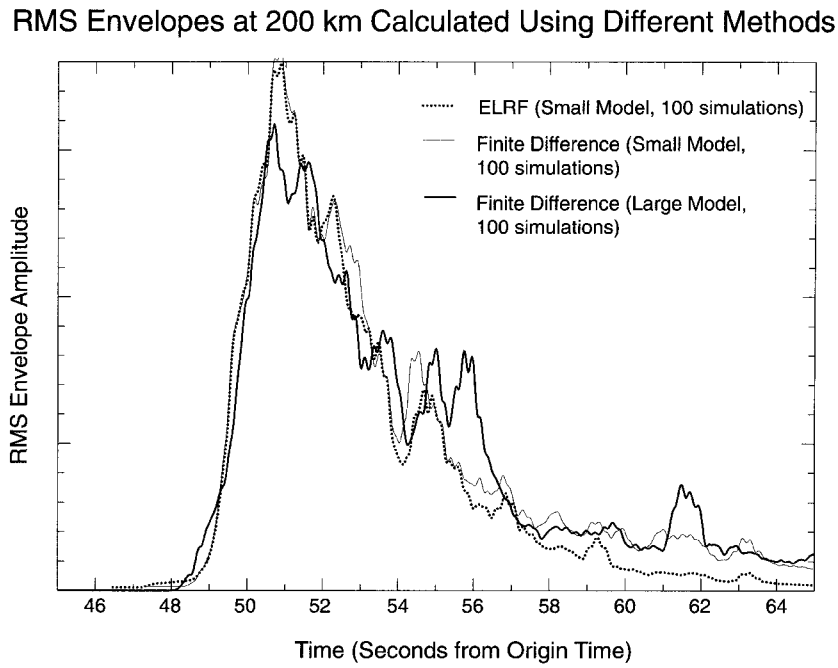

Figure 6. Ensemble-average envelopes at 200 km distance obtained by ELRF for the small model, and by FD for small and large model.

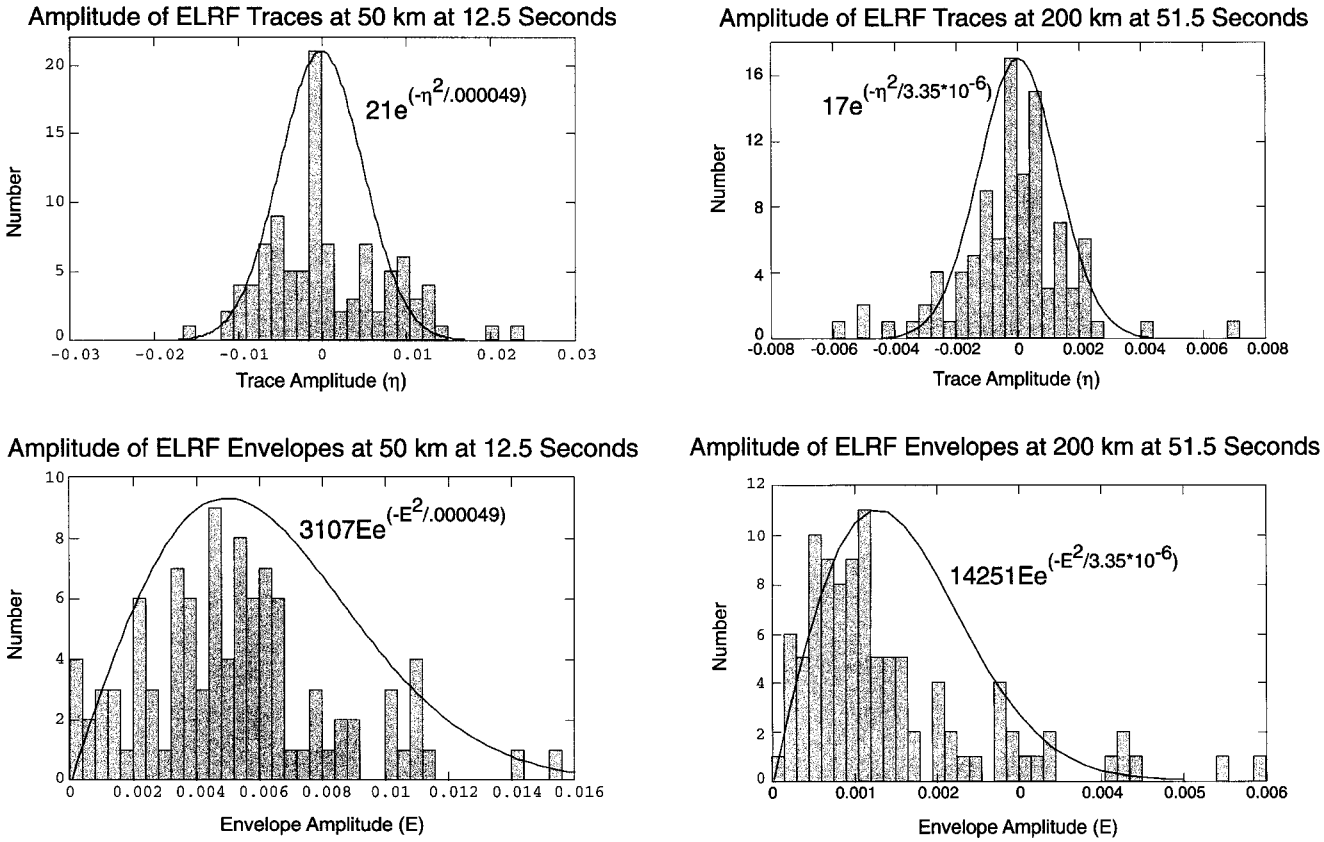

Figure 7. Histograms showing the distributions of wave amplitudes among 100 simulations made using ELRF (top) and envelope amplitudes (lower). Distribution functions defined by (16) and (17) are shown.

parabolic equation for the spatial dependence of the two-frequency mutual coherence function (TFMF), which is the correlation of the wavefield between two locations and two frequencies. We show how the intensity spectral density of the wavefield can be obtained from the two-frequency mutual coherence function. By solving for the intensity spectral density at a given location, we can obtain the temporal dependence of the envelope shape. We use the Markov approximation (see Sato and Fehler, 1998), which was used to study outgoing spherical wave propagation through 3D random media by Shishov (1974) and plane-wave propagation through 3D random media by Lee and Jokipii (1975a,b) and Sreenivasiah *et al.* (1976). The following is a new extension of Shishov's work to 2D.

We define the TMCF at distance r as the correlation of the wavefield between two locations, defined by $r\theta'$ and $r\theta''$, located on a circle of radius r, at different angular frequencies at ω' and ω'' (Ishimaru, 1978)

$$\Gamma_2(\theta',\theta'',r,\omega',\omega'') \equiv \langle U(\theta',r,\omega')U(\theta'',r,\omega'')^*\rangle \quad (18)$$

where angular brackets indicates ensemble average and * indicates complex conjugate. A small part of the circle is the transverse line for outgoing waves from the source. Because we assume that the random media are statistically homogenous, Γ_2 depends only on the difference between locations $r\theta'$ and $r\theta''$.

When the wavelength is smaller than the correlation length of the medium, forward scattering dominates and variations in Γ_2 come from only short offsets in the transverse line. For quasimonochromatic waves having angular frequency centered around $\omega_c = (\omega_1 + \omega_2)/2$, we can derive the equation governing Γ_2 from the parabolic equation (11) for U:

$$\partial_r\Gamma_2 + i\frac{k_d}{2k_c^2r^2}\partial_{\theta_d}^2\Gamma_2 + k_c^2[A(0) - A(r\theta_d)]\Gamma_2 + \frac{k_d^2}{2}A(0)\Gamma_2 = 0 \quad (19)$$

where difference angle $\theta_d = \theta' - \theta''$. We use the center-of-mass coordinate ω_c and define the difference coordinate $\omega_d = \omega_1 - \omega_2$ in the angular-frequency domain, and $k_c = \omega_c/V_0$ and $k_d = \omega_d/V_0$. We note that we used an approximation to evaluate $\langle\xi(\theta', r)U(\theta', r, \omega')U(\theta'', r, \omega'')^*\rangle$ and $\langle\xi(\theta'', r)U(\theta', r, \omega')U(\theta'', r, \omega'')^*\rangle$ on the transverse line. Function A is the longitudinal integral of the autocorrelation function. For the isotropic Gaussian ACF (5), we have

$$A(r\theta_d) \equiv \int_{-\infty}^{\infty} R(x,r\theta_d)dx = \sqrt{\pi}\varepsilon^2 a\,\exp(-r^2\theta_d^2/a^2) \approx \sqrt{\pi}\varepsilon^2 a[1 - (r\theta_d/a)^2] \text{ for } r\theta_d \ll a \quad (20)$$

The derivation of equation (19) is similar to that given in Sato and Fehler (1998, p. 246).

We may interpret the parabolic-wave equation for the mean wavefield $\langle U\rangle$ derived from equation (11) and the similar equation for the average of the higher moment of U (equation (19)) as describing a Markov process since $\langle U\rangle$ and the average of the moment on a layer at $r + \Delta r$ can be calculated from their values on a layer at r. Therefore, our approach is called the Markov approximation (Barabanenkov *et al.,* 1971; Sato and Fehler, 1998).

If we choose Γ_2 to be of the form

$$\Gamma_2 = {}_0\Gamma_2\, e^{-\omega_d^2A(0)r/2V_0^2} \quad (21)$$

where the exponential term represents the phase fluctuation of the outgoing wave, the master equation for ${}_0\Gamma_2$ is given by

$$\partial_r\,{}_0\Gamma_2 + i\frac{k_d}{2k_c^2r^2}\partial_{\theta_d}^2{}_0\Gamma_2 + k_c^2[A(0) - A(r\theta_d)]_0\Gamma_2 = 0 \quad (22)$$

We wish to obtain the intensity spectral density as a function of source-receiver separation. We define the intensity of waves at radial distance r and time t as

$$\begin{aligned} I(r,t) &\equiv \langle u(\theta,r,t)u^*(\theta,r,t)\rangle \\ &\approx \frac{1}{k_cr}\frac{1}{(2\pi)^2}\int_{-\infty}^{\infty}d\omega_c\int_{-\infty}^{\infty}d\omega_d\,\Gamma_2(\theta_d = 0,r,\omega',\omega'')e^{-i\omega_d(t-r/V_0)} \\ &= \frac{1}{2\pi}\int_{-\infty}^{\infty}d\omega_c\hat{I}(r,t;\omega_c) \end{aligned} \quad (23)$$

since $\sqrt{k'k''} \approx k_c$ for quasi-monochromatic waves. The intensity spectral density $\hat{I}$, which is the mean square (MS) of a bandpass-filtered trace of central angular frequency ω_c, is the integral over the difference angular frequency

$$\hat{I}(r,t;\omega_c) = \frac{1}{k_cr}\frac{1}{2\pi}\int_{-\infty}^{\infty}d\omega_d\,\Gamma_2(\theta_d = 0,r,\omega',\omega'')\,e^{-i\omega_d(t-r/V_0)} \quad (24)$$

where the integral kernel is the TMCF. This is the MS envelope.

The contribution of the phase fluctuation (exponential) term of (21) to the intensity spectral density is

$$\frac{1}{2\pi}\int_{-\infty}^{\infty}d\omega_d\,e^{-\omega_d^2A(0)r/2V_0^2}\,e^{-i\omega_d(t-r/V_0)} = \frac{V_0}{\sqrt{2\pi\varepsilon^2ar\sqrt{\pi}}}\,e^{-V_0^2(t-r/V_0)^2/2\sqrt{\pi}\varepsilon^2ar} \quad (25)$$

This term does not influence the broadening of individual

wave packets but shows the wander effect from the statistical averaging of the phase fluctuations of different rays on the transverse line at distance r (Lee and Jokipii, 1975b). To study envelope broadening for a single realization, we need to find ${}_0\Gamma_2$ that solves (22), and we should use ${}_0\Gamma_2$ instead of Γ_2 in (24). To find the average of many realizations as shown in the following, we use Γ_2 given by using (21) in (24).

MS Envelope of Outgoing Cylindrical Waves for an Impulsive Source

For outgoing waves from an impulsive source in a homogeneous medium ${}_0\Gamma_2 = C^2/2\pi$, where the constant C has the dimension of U, we have the intensity spectral density $\hat{I}(r, t; \omega_c) = (C^2/k_c)\,\delta(t - r/V_0)/2\pi r$, which represents a wavelet propagating outward with velocity V_0. For a random medium, we may put the initial condition at $r = 0$ as

$$ {}_0\Gamma_2(\theta_d,\, r = 0, \omega', \omega'') = C^2/2\pi \tag{26} $$

The contribution to the MS envelope at a long travel distance comes from a small transverse distance. In the case of the Gaussian ACF, substituting (20) into (22), we explicitly write the equation for ${}_0\Gamma_2$ as

$$ \partial_r\, {}_0\Gamma_2 + i\,\frac{k_d}{2k_c^2 r^2}\,\partial_{\theta_d}^2\, {}_0\Gamma_2 + \frac{\sqrt{\pi}\varepsilon^2 k_c^2 r^2 \theta_d^2}{a}\, {}_0\Gamma_2 = 0 \tag{27} $$

It is easier to work with equation (27) in nondimensional form. We thus introduce the nondimensional transverse distance χ scaled by the transverse correlation distance $a_\perp = \sqrt{a/\sqrt{\pi}\varepsilon^2 r_0 k_c^2}$ and longitudinal distance τ scaled by travel distance r_0 as

$$ r = r_0\,\tau \text{ and } r_0\,\theta_d = a_\perp \chi \tag{28} $$

We define the characteristic wavenumber as

$$ k_M \equiv \frac{2k_c^2 a_\perp^2}{r_0} = \frac{2a}{\sqrt{\pi}\varepsilon^2 r_0^2} \tag{29} $$

Then, the nondimensional form of (27) becomes

$$ \partial_\tau\, {}_0\Gamma_2 + i\,\frac{k_d}{k_M\,\tau^2}\,\partial_\chi^2\, {}_0\Gamma_2 + \tau^2\chi^2\, {}_0\Gamma_2 = 0 \tag{30} $$

Under the initial condition ${}_0\Gamma_2(\tau = 0, \chi) = C^2/2\pi$, we want to find the TMCF at distance r_0 and at difference angle $\theta_d = 0$ that is, ${}_0\Gamma_2\,(\tau = 1, \chi = 0)$. First, we assume that the solution has the following form:

$$ {}_0\Gamma_2(\tau, \chi) = \frac{e^{\nu(\tau)\tau^2\chi^2}}{w(\tau)} \tag{31} $$

Then, (30) reduces to

$$ \left[\frac{d\nu}{d\tau} + \frac{2}{\tau}\,\nu + 4i\left(\frac{k_d}{k_M}\right)\nu^2 + 1\right]\tau^2\chi^2 + \left[2i\left(\frac{k_d}{k_M}\right)\nu - \frac{1}{w}\,\frac{dw}{d\tau}\right] = 0 \tag{32} $$

Each term in brackets in (32) must be zero to satisfy the equation regardless of χ. The differential equation for $\nu(\tau)$ is a Riccati equation. Using the initial condition, $\nu(0) = 0$ and $w(0) = 2\pi/C^2$, we have

$$ \nu(\tau) = \frac{1}{s_0}\cot s_0\tau - \frac{1}{s_0^2\tau} \text{ and } w(\tau) = \frac{2\pi}{C^2}\sqrt{\frac{\sin s_0\tau}{s_0\tau}} \tag{33} $$

where $s_0 = 2e^{\pi i/4}\sqrt{k_d/k_M}$. Finally we obtain

$$ {}_0\Gamma_2(\tau, \chi) = \frac{C^2}{2\pi}\sqrt{\frac{s_0\tau}{\sin s_0\tau}}\exp\left[\left(\frac{\tau^2}{s_0}\cot s_0\tau - \frac{\tau}{s_0^2}\right)\chi^2\right] \tag{34} $$

At $\tau = 1$ and $\chi = 0$, (34) becomes

$$ {}_0\Gamma_2(\tau = 1, \chi = 0) = \frac{C^2}{2\pi}\sqrt{\frac{2e^{\pi i/4}\sqrt{k_d/k_M}}{\sin(2e^{\pi i/4}\sqrt{k_d/k_M})}} \tag{35} $$

Substituting (35) and (24), we get the intensity spectral density as

$$ \hat{I}(r_0, t; \omega_c) = \left(\frac{C^2}{k_c}\right)\frac{1}{2\pi r_0}\,\frac{1}{2\pi} \int_{-\infty}^{\infty} d\omega_d \sqrt{\frac{2e^{\pi i/4}\sqrt{\omega_d/V_0 k_M}}{\sin(2e^{\pi i/4}\sqrt{\omega_d/V_0 k_M})}}\, e^{-i\omega_d(t - r_0/V_0)} \tag{36} $$

Equation (36) corresponds to the MS envelope or intensity spectral density for a single realization when the initial condition is $\hat{I}(r, t; \omega_c) = (C^2/k_c)\,\delta(t - r/V_0)/2\pi r$ near the source ($r \approx 0$).

Therefore, for a unit radiation of intensity spectral density $\delta(t - r/V_0)/2\pi r$ at the source, replacing $C^2/k_c \to 1$, we have

$$ \hat{I}(r_0, t) = \frac{1}{2\pi r_0}\,\frac{1}{2\pi}\int_{-\infty}^{\infty} d\omega_d \sqrt{\frac{2e^{\pi i/4}\sqrt{\omega_d/V_0 k_M}}{\sin(2e^{\pi i/4}\sqrt{\omega_d/V_0 k_M})}}\, e^{-i\omega_d(t - r_0/V_0)} \tag{37} $$

which is independent of central frequency. This is due to the

choice of Gaussian ACF for the random media. When we scale the time and angular frequency by using the characteristic time

$$t_M \equiv \frac{1}{V_0 k_M} = \frac{\sqrt{\pi}}{2V_0}\frac{\varepsilon^2}{a} r_0^2 \tag{38}$$

as $\bar{\omega}_d = t_M \omega_d$, we may rewrite (37) as

$$\hat{I}(r_0,t) = \frac{1}{t_M}\frac{1}{2\pi r_0}\frac{1}{2\pi}\int_{-\infty}^{\infty} d\bar{\omega}_d \sqrt{\frac{2e^{\pi i/4}\sqrt{\bar{\omega}_d}}{\sin(2e^{\pi i/4}\sqrt{\bar{\omega}_d})}}\, e^{-i\bar{\omega}_d(t-r_0/V_0)/t_M} \tag{39}$$

We can numerically evaluate (39) by using an FFT. Note that the envelope characteristics are a function of the scaled time t_M and thus depend on the ratio of the mean squared velocity fluctuation to correlation length ε^2/a.

Envelopes in Random Media

Figure 8 shows the temporal change in the intensity spectral density including the geometrical spreading correction for the Gaussian ACF as given by (39). This plot is calculated from ${}_0\Gamma_2$ by using a FFT of 256 points, so it should be compared with a single realization. The peak amplitude of 3.2 occurs at time 0.12 t_M after the direct arrival, the half-maximum arrival occurs at 0.29 t_M, and the quarter maximum, which corresponds to the half maximum of the rms intensity spectral density, is at 0.45 t_M. Since t_M in (38) is proportional to the square of the propagation distance, the envelope width for a delta function-like source is proportional to the square of travel distance. We note $\int_{r_0/V_0}^{\infty} \hat{I}(r_0, t)2\pi r_0 dt = 1$, which means that all the energy radiated from the origin passes through a circle of radius r_0 since we disregard backward scattering in the derivation.

To calculate the intensity spectral density, which corresponds to MS envelope, for the 2 Hz Ricker wavelet source, we multiply the TMCF by the Fourier spectra of the Ricker wavelet's square trace before the Fourier transform. As predicted, the envelope width for the Ricker wavelet source is larger than that for the delta function source, and the height of envelope for the Ricker wavelet source is smaller than that for the delta function source. In Figure 9, we plot the temporal change in the intensity spectral density at distance $r_0 = 200$km. Solid and broken curves are for a delta function-like source and for a 2-Hz Ricker wavelet source, respectively. Envelopes having narrow peaks are for the single realization (${}_0\Gamma_2$) given by (39) and those having broad peaks are for the ensemble average (Γ_2) including the wander effect.

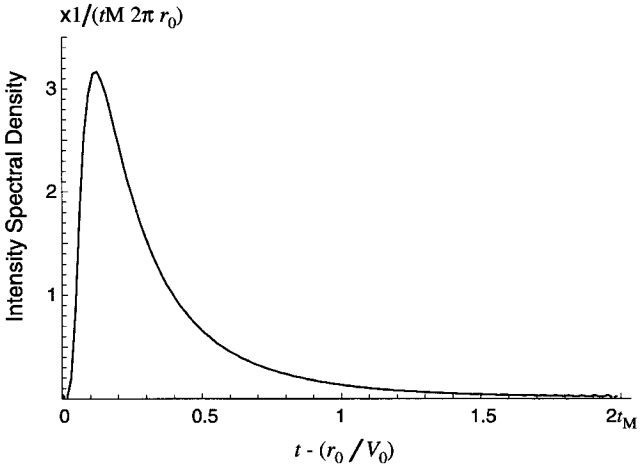

Figure 8. Temporal change in the intensity spectral density at distance r_0 for single realization (${}_0\Gamma_2$) in 2D random media characterized by the Gaussian ACF, where t_M is the characteristic time.

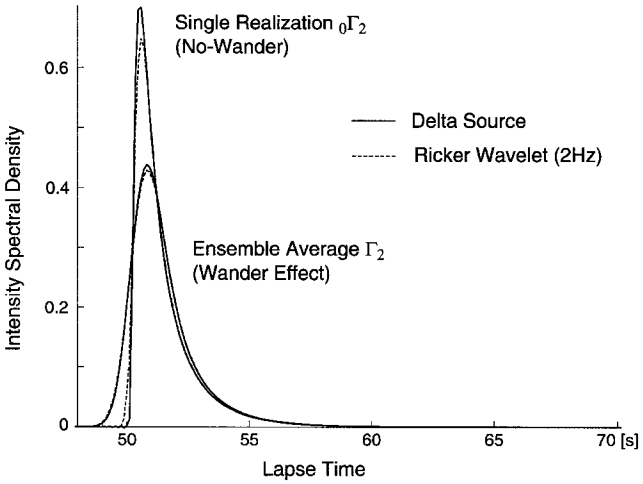

Figure 9. Temporal change in the intensity spectral density based on the Markov approximation in 2D random media ($V_0 = 4$ km/sec) characterized by the Gaussian ACF ($\varepsilon = 0.05$ and $a = 5$ km) at a distance of 200 km: solid and broken curves are for a delta function-like source and for a 2 Hz Ricker wavelet source, respectively. Envelopes having narrow peaks are for the single realization (${}_0\Gamma_2$) and those having broad peaks are for the ensemble average (Γ_2) including wander effect, respectively.

Discussion

Comparison of Envelopes Calculated Using Various Methods

Figure 10 shows a comparison of rms envelopes for a 2-Hz Ricker wavelet source in a 2D random media ($V_0 = 4$ km/sec) characterized by the Gaussian ACF ($\varepsilon = 0.05$ and $a = 5$ km) for travel distance ranging from 50 km to 200 km. Plotted are the analytical simulation based on the Mar-

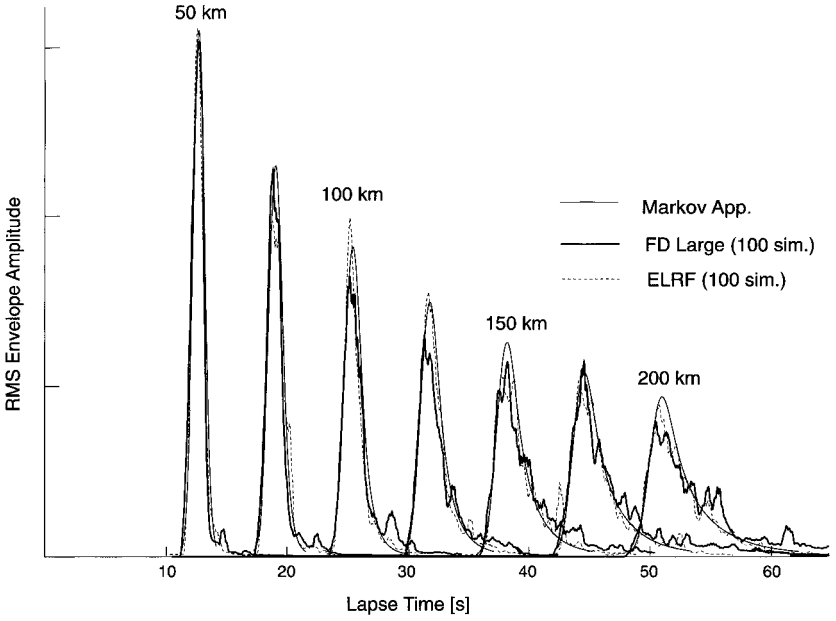

Figure 10. Comparison of RMS envelopes for a 2Hz Ricker wavelet source in 2D random media ($V_0 = 4$ km/sec) characterized by the Gaussian ACF ($\varepsilon = 0.05$ and $a = 5$ km) at distances from 50 km to 200 km: solid curves, analytical solution of the Markov approximation; gray solid curves, rms envelopes of 100 simulations using FD; broken gray curves, rms envelopes of 100 simulations using ELRF.

kov approximation (fine solid curves) with the ensemble average rms envelopes calculated by the ELRF method (broken curves) and the ensemble average rms envelope by the FD method for the large model (thick solid curves). All the traces are smoothed over a .32-sec time window. An excellent coincidence between the analytical envelope and the ELRF envelope is reasonable, since both syntheses calculate scattering in a narrow cone around the forward direction and neglect backward scattering. The coda excitation level for the FD envelope is larger than the analytical envelope (see coda levels of the envelope at 200 km at lapse time of 60 sec). This larger coda is caused by large angle scattering, which is mostly caused by short wavelength components of random inhomogeneities. The FD method includes the contribution of large angle scattering, which is neglected in the Markov approximation.

Comparison of Modeling Techniques

We have found that the ELRF modeling technique provides reliable waveforms for models where forward scattering dominates. The ELRF waveforms compare well with FD waveforms for several cycles between the first arrival and some later time where multiple scattering begins to become important. Since the ELRF is a significantly faster modeling technique, it can be a valuable tool for modeling initial arrival packets for waves that have propagated through complex media. The ELRF method provides a mean envelope shape that is in excellent agreement with that calculated using the Markov approximation. The envelopes obtained using the Markov and ELRF approaches differ from the FD envelopes beginning after the time that the envelope reaches its peak. To obtain a complete understanding of the scattering phenomena, we must ultimately use models that include all wave phenomena.

The ELRF and FD methods allow us to easily explore individual waveforms and ensemble-average envelopes for a range of models. Since individual waveforms are calculated, we can investigate the distribution of waveform shapes that contribute to the ensemble-average envelope and thus place some bounds on the statistics of the envelope shape.

Factors that Influence Envelope Shapes

We have studied envelope broadening for the case of a Gaussian correlation function. The choice of a Gaussian ACF was made to facilitate comparison between numerical modeling methods and the Markov approximation. Factors such as variation in the ratio of correlation length to the dominant wavelength and the MS velocity fluctuation will influence the waveform shape. The Markov approximation provides a guide to predict the influence of these factors. Our results indicate that the predictions made by the Markov approximation are reliable for the case of small velocity fluctuation ($\varepsilon < 0.05$). We cannot draw conclusions about cases where fluctuations are larger. When fluctuation increases or the ratio of wavelength to correlation length increase, forward scattering becomes less dominant and the Markov approximation is unreliable because the wide-angle scattering dominates and the parabolic equation (11) no longer adequately describes the wavefield. The heterogeneity of the Earth may be more appropriately described using a Von Kármán or exponential ACF because they contain a wider range of sizes of heterogeneities. In these cases, we may expect that the envelope broadening becomes frequency-dependent, which

is different from the Gaussian case (see Sato and Fehler, 1998, p. 252).

We have not attempted to investigate the influence of anelastic attenuation on envelope shapes. We anticipate that attenuation will decrease the later portion of the predicted envelopes.

Conclusion

We have investigated the propagation of waves radiated from a point source in 2D random media, whose stochastic character is given by a Gaussian ACF, by discarding phase information and investigating the envelope shape. We compared the ensemble average of rms envelopes based on wave simulations by using the FD method with the analytical rms envelopes based on the Markov approximation. We found a good coincidence between them. For the analytical envelope, the envelope characteristics such as peak delay and half-width are given by the statistical parameters of the velocity inhomogeneity: the key parameter is the ratio of MS fractional fluctuation to correlation distance.

When we carefully examine the difference between FD envelopes and analytical envelopes, we find that the FD envelopes have a larger coda excitation. We may interpret this difference as resulting from large angle scattering which is mostly caused by short wavelength components of random inhomogeneities. It is left for us to explain these differences by extending the analytical approach to adopt large angle scattering.

We find that the distribution of waveform and envelope amplitudes is consistent with that predicted for waveforms that are composed of a sum of waves having the same frequency but differing phase. This result is in agreement with the concept that waveforms dominated by forward scattering of narrow-bandwidth waves may be considered to be a superposition of waves of differing phases arriving at an observation point.

Acknowledgments

We gratefully thank Editor Robert Nowack and two reviewers, whose comments helped us to improve the presentation of this work. Work at Los Alamos National Laboratory was supported by the United States Department of Energy Office through contract W-7405-ENG-36 from the Office of Basic Energy Sciences headed by Nick Woodward. This is Contribution Number 13 of the Los Alamos Seismic Research Center.

References

Aki, K. (1969). Analysis of seismic coda of local earthquakes as scattered waves, *J. Geophys. Res.* **74,** 615–631.

Barabanenkov, Yu. N., Yu. A. Kravtsov, S. M. Rytov, and V. I. Tamarskii (1971). Status of the theory of propagation of waves in randomly inhomogeneous medium, *Soviet Phys. Usp.* (Eng. Trans.) **13,** 551–680, 1971.

Chernov, L. A. (1960). Wave Propagation in a Random Medium (Engl. trans. by R. A. Silverman), McGraw-Hill, New York.

Dainty, A. M., and M. N. Toksöz (1990). Array analysis of seismic scattering, *Bull. Seism. Soc. Am.* **80,** 2242–2260.

Der, A. Z., M. E. Marshall, A. O'Donnell, and T. W. McElfresh (1984). Spatial coherence structure and attenuation of the Lg phase, site effects, and interpretation of the Lg coda, *Bull. Seism. Soc. Am.* **74,** 1125–1147.

Flatté, S. M., and R. S. Wu (1988). Small-scale structure in the lithosphere and asthenosphere deduced from arrival time and amplitude fluctuations at NORSAR, *J. Geophys. Res.* **93,** 6601–6614.

Frankel, A., and R. W. Clayton (1986). Finite-difference simulations of seismic scattering: Implications for the propagation of short-period seismic waves in the crust and models of crustal heterogeneity, *J. Geophys. Res.* **91,** 6465–6489.

Gusev, A. A., and I. R. Abubakirov (1996). Simulated envelopes of non-isotropically scattered body waves as compared to observed ones: another manifestation of fractal heterogeneity, *Geophys. J. Int.* **127,** 49–60.

Higdon, R. L. (1991). Absorbing boundary conditions for elastic waves, *Geophysics* **56,** 231–241.

Holberg, O. (1987). Computational aspects of the choice of operator and sampling interval for numerical differentiation in large-scale simulation of wave phenomena, *Geophys. Prospect.,* **35,** 629–655.

Huang, L-J., and M. Fehler, (1998). Accuracy analysis of the split-step Fourier propagator: Implications for seismic modeling and migration, *Bull. Seism. Soc. Am.* **88,** 18–29.

Huang, L-J., M. Fehler, P. Roberts, and C. C. Burch (1999). Extended local Rytov Fourier migration method, *Geophysics* **64,** 1535–1545.

Ikelle, L. T., S. K. Yung, and F. Daube (1993). 2-D random media with ellipsoidal autocorrelation functions, *Geophysics* **58,** 1359–1372.

Ishimaru, A. (1978). *Wave Propagation and Scattering in Random Media,* Vols. 1 and 2, Academic Press, New York.

Jensen, F., W. Kuperman, M. Porter, and H. Schmidt (1994). *Computational Ocean Acoustics,* American Institute of Physics Press, New York.

Landon, V. (1941). The distribution of amplitude with time in fluctuation noise, *Proc. I.R.E.* **29,** 50–55.

Landon, V. (1942). Discussion on the distribution of amplitude with time in fluctuation noise, *Proc. I.R.E.* **30,** 425–429.

Lee, L. C., and J. R. Jokipii (1975a). Strong scintillation in astrophysics. I. The Markov approximation, its validity and application to angular broadening, *Astrophys. J.* **196,** 695–707.

Lee, L. C., and J. R. Jokipii (1975b). Strong scintillations in astrophysics. II. A theory of temporal broadening of pulses, *Astrophys. J.* **201,** 532–543.

Müller, G., M. Roth, and M. Korn (1992). Seismic wave traveltimes in random media, *Geophys. J. Int.* **110,** 29–41.

Obara, K., and H. Sato (1995). Regional differences of random inhomogeneities around the volcanic front in the Kanto-Tokai area, Japan, revealed from the broadening of *S* wave seismogram envelopes, *J. Geophys. Res.* **100,** 2103–2121.

Rayleigh, Lord (1880). On the resultant of a large number of vibrations of the same pitch and of arbitrary phase, *Phil. Mag.* **10,** 73–78.

Roth, M., G. Müller, and R. Snieder (1993). Velocity shift in random media, *Geophys. J. Int.* **115,** 552–563.

Sato, H. (1982). Amplitude attenuation of impulsive waves in random media based on travel time corrected mean wave formalism, *J. Acoust. Soc. Am.* **71,** 559–564.

Sato, H. (1989). Broadening of seismogram envelopes in the randomly inhomogeneous lithosphere based on the parabolic approximation: southeastern Honshu, Japan, *J. Geophys. Res.* **94,** 17,735–17,747.

Sato, H., and M. Fehler (1998). *Seismic Wave Propagation and Scattering in the Heterogeneous Earth,* AIP Press/Springer Verlag, New York, 308 pp.

Scherbaum, F., and H. Sato (1991). Inversion of full seismogram envelopes based on the parabolic approximation: estimation of randomness and attenuation in southeast Honshu, Japan, *J. Geophys. Res.* **96,** 2223–2232.

Shapiro, S., and P. Hubral (1999). Elastic Waves in Random Media, Fundamentals of Seismic Stratographic Filtering, Springer-Verlag, Berlin, 191 pp.

Shapiro, S. A., and G. Kneib (1993). Seismic attenuation by scattering: theory and numerical results, *Geophys. J. Int.* **114,** 373–391.

Shishov, V. I. (1974). Effect of refraction on scintillation characteristics and average pulse shape of pulsars, *Sov. Astron.* **17,** 598–602.

Sreenivasiah, I., A. Ishimaru, and S. T. Hong (1976). Two-frequency mutual coherence function and pulse propagation in a random medium: An analytic solution to the plane wave case, *Radio Sci.* **11,** 775–778.

Stoffa, P. L., J. T. Fokkema, R. M. L. Freire, and W. P. Kessinger (1990). Split-step Fourier migration, *Geophysics* **55,** 410–421.

Wagner, G. S. (1997). Regional wave propagation in southern California and Nevada: Observations from a three-component seismic array, *J. Geophys. Res.* **102,** 8285–8311.

Los Alamos Seismic Research Center
MS D443
Los Alamos National Laboratory
Los Alamos, New Mexico 87545
fehler @lanl.gov; ljh@lanl.gov
(M. F., L. J. H.)

Department of Geophysics
Graduate School of Science
Tohoku University
Aoba-ku, Sendai-shi, 980-8578, Japan
sato @zisin.geophys.tohoku.ac.jp
(H. S.)

Manuscript received 21 October 1999.